NANO MICRO small

Supporting Information

for *Small,* DOI: 10.1002/smll.202101743

Ultrasensitive Multiparameter Phenotyping of Rare Cells Using an Integrated Digital-Molecular-Counting Microfluidic Well Plate

Shiuan-Haur Su, Yujing Song, Michael W. Newstead, Tao Cai, MengXi Wu, Andrew Stephens, Benjamin H. Singer, and Katsuo Kurabayashi**

WILEY-VCH

Supporting Information

Ultrasensitive multiparameter phenotyping of rare cells using an integrated digital-molecular-counting microfluidic well plate

Shiuan-Haur Su, Yujing Song, Michael W. Newstead, Tao Cai, MengXi Wu, Andrew Stephens, Benjamin H. Singer and Katsuo Kurabayashi**

S.-H. Su, Y. Song, T. Cai, M. Wu, A. Stephens, Prof. K. Kurabayashi
Department of Mechanical Engineering, University of Michigan, Ann Arbor MI, 48109 USA
E-mail: katsuo@umich.edu

M.W. Newstead, Prof. B.H Singer
Department of Internal Medicine, Division of Pulmonary and Critical Care Medicine, University of Michigan, Ann Arbor, MI, 48109, USA
Email:singerb@med.umich.edu

Prof. K. Kurabayashi
Department of Electrical Engineering and Computer Science, University of Michigan, Ann Arbor, MI, 48109 USA
Email: katsuo@umich.edu

Prof. B.H. Singer and Prof. K. Kurabayashi
Michigan Center for Integrative Research in Critical Care, University of Michigan, Ann Arbor, MI, 48109, USA
Email: singerb@med.umich.edu, katsuo@umich.edu

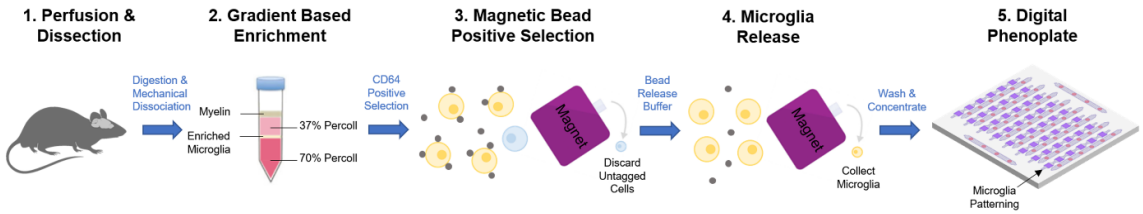

Figure S1 Microglia isolation and enrichment method. (1) Euthanized mice were perfused. Their brains were dissected and triturated to single cell suspensions through enzymatic digestions and gentle mechanical dissociations (2) Microglia were enriched with a gradient-based isolation process using 37% and 70% Percoll layers to eliminate the myelin and red blood cells in the sample tube. (3) Enriched microglia were then stained with PE or biotin labeled CD64 antibodies (depending on the releasable bead kit used) Magnetic beads bound to the labeled microglia were retained in the tube. Unlabeled cells were discarded. (4) A bead release buffer was then added to the sample. The beads were cleaved from the microglia. (5) Purified microglia were then collected, concentrated and loaded onto the assay chambers of the dPP chip for cellular phenotyping

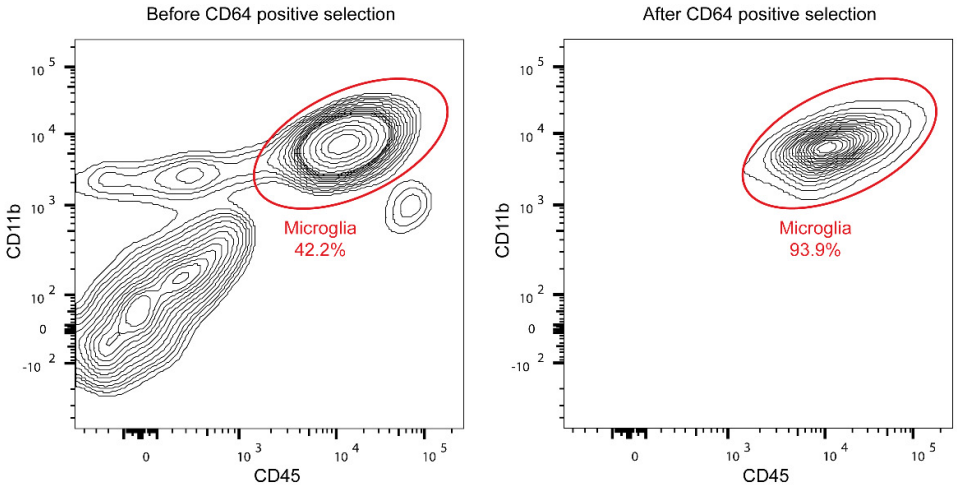

Figure S2 Microglia purity assessed by flow cytometry before and after CD64 positive selection using releasable magnetic beads. Microglia were identified as either CD45mid/CD11b+or CD45hi/CD11b+. The CD64 positive selection process eliminates cells that express Ly6C, which include some infiltrating monocytes and neutrophils in the sample. The microglia purity achieved by the CD64 positive selection was 93.9% while it was 42.2% prior to the selection.

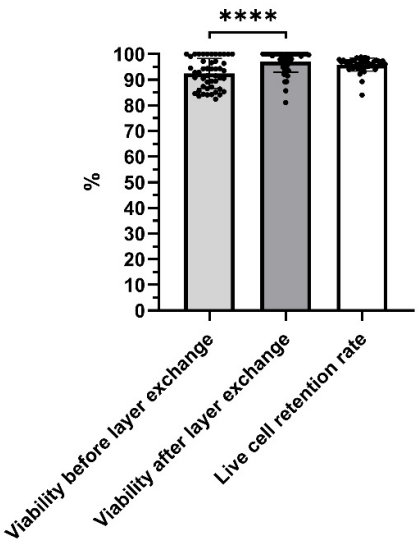

Figure S3 RAW 264.7 cell viability change and live cell retention rate after the PDMS channel layer exchange process. The viability was assessed by the fraction of the number of green-fluorescent calcein emitting cells to the total cell count determined by a brightfield image. A paired t test analysis indicates an increased viability rate after the replacement of PDMS channel layer 1 with PDMS channel layer 2 with $p < 0.0001$. This is possibly because dead cells were less adherent than healthy live cells and therefore likely removed during the layer changing process. The live cell retention rate of ~95% was assessed by the fraction of the number of green fluorescence emitting cells counted after the layer exchange to the number of green fluorescence emitting cells counted prior to the layer exchange.

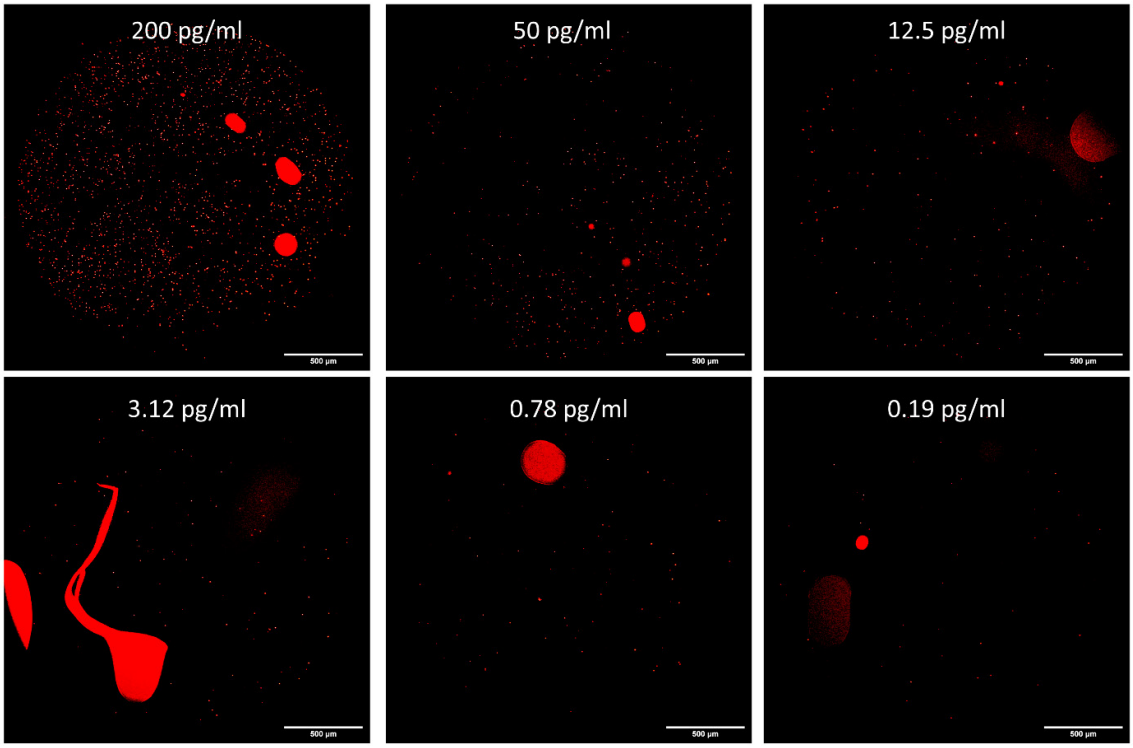

Figure S4 Representative snapshot images of enzyme active "On" bead microwells in the digital sensor array patch (66,724 wells per patch) for various concentrations of TNF-α. For clear visualization, images of 4000×4000 pixels were cropped from the original raw images of 6000×4000 pixels with 70% brightness enhancement and 70% contrast enhancement. All scale bars are 500 μm. The large bright spots in the images are defects caused by debris or local failure of oil sealing. They are eliminated from signal counting by our machine learning-based image processing algorithm detailed in our previous work. [43]

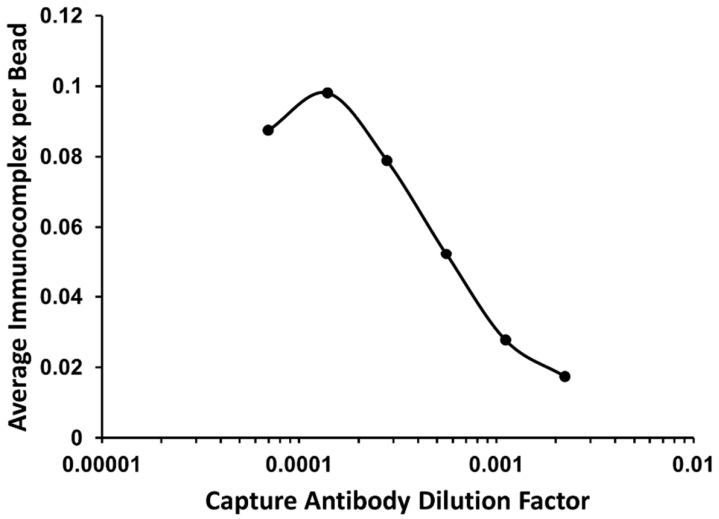

Figure S5 Digital immunosensor-based assay signal for 100pg mL^{-1} TNF-α resulting from various dilution factors of capture antibody concentrate from a commercial ELISA kit. In our assay format, the capture antibodies were sandwiched between the antigen analytes and the anti-hamster IgG secondary antibodies on the beads. We observed that providing excess capture antibodies yielded a significant decrease in the signal strength possibly due to the saturation of anti-IgG secondary antibody binding sites on the beads by empty capture antibodies. The bead saturation causes fewer antibodies capturing the antigen molecule in the suspension medium to be bound to the beads later during the reaction, resulting in a small signal-to-noise ratio. On the other hand, a lack of capture antibodies loaded at a low concentration leads to a reduced sensor dynamic range with the insufficient ability to capture antigens from the sample. From the data shown here, we selected the dilution factor to be ~ 1/7200 to achieve the best assay dynamic range and sensor sensitivity. The concentration of the capture antibodies loaded at this dilution factor is expected to match the total number of the capture antibodies with the total anti IgG capture sites on all beads in the digital sensor arrays.

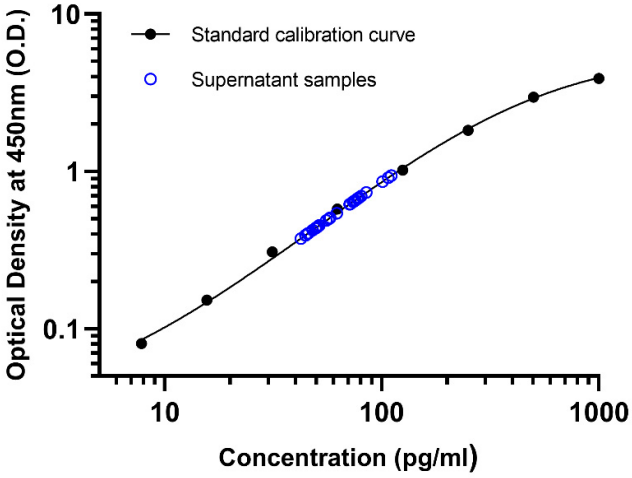

Figure S6 Commercial ELISA (Invitrogen™) standard curve for TNF-α and results of the ELISA measurements of RAW 264.7 cell-secreted TNF-α in a cell culture supernatant. The LOD of the ELISA kit was 8pg mL^{-1}. All supernatant samples measured were within the assay range of the ELISA kit.

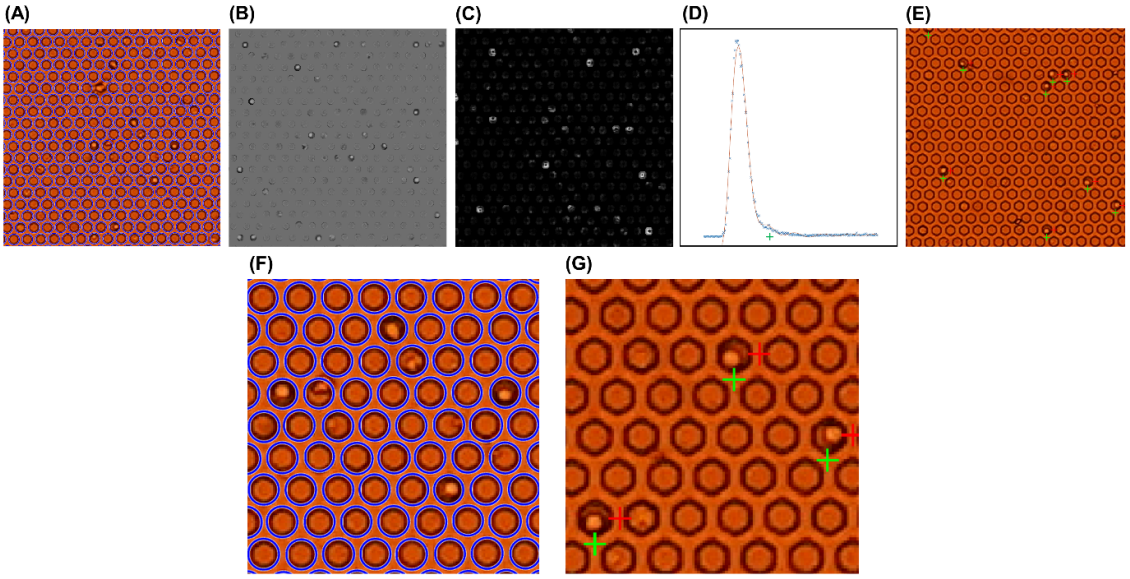

Figure S7 MATLAB computer vision cell recognition and counting code. Representative images were zoomed in and cropped at different locations of the raw image for visualization of the process (A) Microwells were first detected (blue circles) using the Circular Hough Transform (CHT)-based algorithm, which is robust in finding circles at the presence of noise, debris occlusion, and non-uniform illumination. (B) The detected circles were then used as a mask for image preprocessing. (C) A range filter function was first used to detect the microwells in the image texture. (D) The range value distribution for all microwells was plotted and generated for each raw image, and a threshold (green cross in the figure) was individually assigned to provide robustness for out-of-focus images (E) Cell recognition and counting in each microwell were performed by combining the multiple layers of image-segmenting methods based on the range value, intensity distribution, and edge detection to

provide accurate and consistent results. (F) Zoomed-in image of Figure S7A for better visualization of the detected wells marked in blue circles. (G) Zoomed-in image of Figure S7E for better visualization of wells that were recognized to be occupied by a single cell. The red crosses were recognitions solely based on range value thresholding and the green crosses were the recognitions that implemented all other image-segmenting metrics on top of the range thresholding and were taken as the final accurate result.

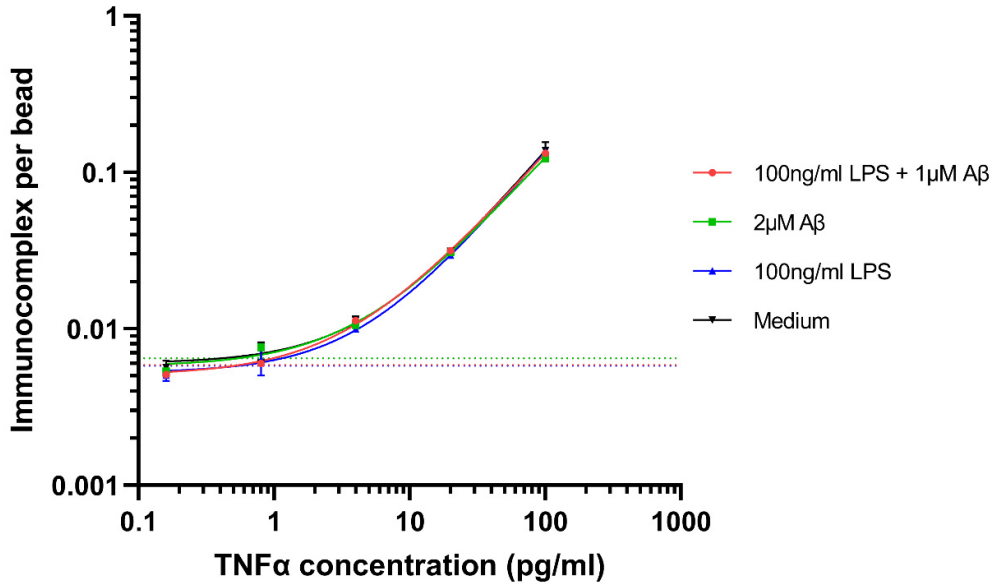

Figure S8 4 integrated digital immunosensor standard curves for TNF-α in 100ng mL^{-1} LPS + 1 μM Aβ, 2 μM Aβ, 100ng mL^{-1} LPS, and cell culture medium. The data points were fitted with a 4PL curve. The colored dotted lines represent 3σ above the blank signal level in the corresponding same color stimulant in the legend. The limit of detection (LOD) in 100ng mL^{-1} LPS + 1 μM Aβ, 2 μM Aβ, 100ng mL^{-1} LPS, and cell culture medium was calculated to be 0.565 pg mL^{-1}, 0.548 pg mL^{-1}, 0.530 pg mL^{-1} and 0.397 pg mL^{-1} , respectively. There was no significant loss of sensitivity or signal differences between different stimulants and all of our cellular secretory phenotyping data presented are well above these LODs.